

Figure 1. NEUROBOT, a medical parallel manipulator developed for neuro surgeries.

In applying such a system in the clinic operations, kinematic calibration of the system must be carried out to improve the accuracy of motion control. For most of the parallel manipulator systems, their calibration tends to be conducted in two stages: first is the manipulator self-calibration and then the base/tool calibration. The manipulator self-calibration deals with the kinematic parameter identification for the coordinate from base to mobile platform.⁸ It can be conducted with either external measuring devices like theodolite⁹ and linear variable differential transformer (LVDT),¹⁰ or adding extra sensors to the system.¹¹

On the other hand, the base and tool calibration concerns the errors in both base and tool (end-effector) transformations.^{12–14} In general, there are at least two factors that contribute to the errors. One factor is related to the base and tool installation. For parallel manipulator systems, the manipulator must be installed in such a way that its base platform is mounted on a support, either mobile or fixed, and a certain tool is attached to the mobile platform. This definitely introduces installation-associated errors which may include the connecting parts' manufacturing tolerance, link offset, and assembly error. The other factor is the inaccessibility of the origins of both base and mobile platform coordinate systems. The origins are either the geometric center or the centroid of the platforms, which are located inside the rigid body and cannot be measured directly. What we can do is only to provide initial estimations for them.

In this paper, a method of base and tool calibration is developed for our medical parallel manipulator system. The calibration is carried out with an op-

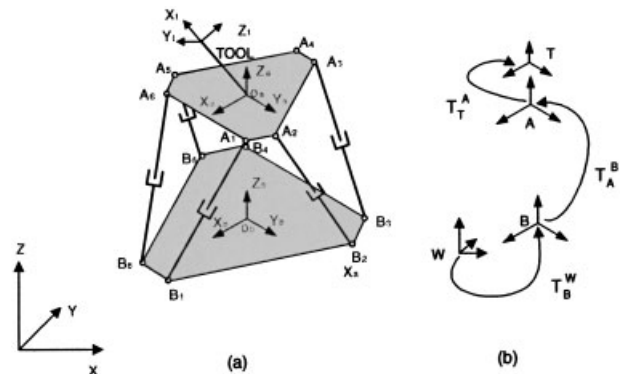


Figure 2. (a) Coordinate frames for medical robot calibration, and (b) the relationships among all transformations.

tical position sensor, OPTOTRAK 3020 (product of Northern Digital Inc., Canada). An error model for the base and tool transformation was first constructed. The pose measurement technology with OPTOTRAK 3020 was then described. Lastly, the simulation and experiment results were presented to demonstrate the effectiveness of the method.

2. PROBLEM FORMULATION

The parallel manipulator with an end-effector attached to its mobile platform can be abstracted as a model shown in Figure 2. In the model, a hexapod has legs mounted on the base plate at ball joints B_1 to B_6 , arranged in pairs, B_1 – B_6 , B_2 – B_3 and B_4 – B_5 . The set of all six legs is arranged symmetrically on the base, on a circle with a radius r_b . For the six joints A_1 to A_6 on the mobile platform, the geometric configuration is similar to that of base platform.

Two coordinate frames are set up for the parallel manipulator. The fixed frame $B\{X_b, Y_b, Z_b\}$ is located in the center of the base platform. The mobile frame $A\{X_a, Y_a, Z_a\}$ is located in the center of mobile platform. In addition, we also set up two other frames for the system. One is attached to the tool (end-effector), called frame T . Another is the world frame W which is a fixed reference frame. The establishment of frames T and W will be described in Section 5.1.

The homogeneous transformation matrix relating the manipulator's tool frame to the world frame is

$$T_T^W = T_B^W T_A^B T_T^A. \quad (1)$$

In Eq. (1), T_A^B is a function of six pose parameters:

$$T_A^B = \text{Tra}(x,y,z)\text{Rot}(x,\theta_x)\text{Rot}(y,\theta_y)\text{Rot}(z,\theta_z), \quad (2)$$

where $\text{Tra}(x,y,z)$ is the homogeneous matrix corresponding to a translation of (x,y,z) , $\text{Rot}(x,\theta_x)$ is the matrix describing a rotation of θ_x about X axis and similarly $\text{Rot}(y,\theta_y)$ and $\text{Rot}(z,\theta_z)$ for Y and Z axes, respectively. By self-calibration, T_A^B can be identified with enough accuracy. For matrices T_B^W and T_T^A , they are both fixed and not varied with pose parameters. However, as stated in Section 1, we can only give estimations of T_B^W and T_T^A due to the inaccessibility of origins of frame A and B.

In obtaining an accurate value of these two matrices, an existing method is to rewrite Eq. (1) into the form of $T_T^W(T_T^A)^{-1} = T_B^W T_A^B$ (i.e., $AX=YB$),¹⁴ which can be solved through quaternion algebra. In this paper, the solution of two matrices is derived by differential approach, i.e., the accurate value is obtained by calculating the measuring error. Obviously, this method is more straightforward and easy to understand for parallel manipulators.

3. ERROR MODEL

As stated in Section 2, T_A^B is regarded to be accurate in the stage of tool and base calibration in that it has been self-calibrated. Therefore, we can consider only the errors of transformation of T_B^W and T_T^A . Let dT denote an error matrix which is the deviation from the expected position related to a transformation T . For T_T^W . The following equation exists:

$$T_T^W + dT_T^W = (T_B^W + dT_B^W)T_A^B(T_T^A + dT_T^A). \quad (3)$$

Expanding the right side of Eq. (3) and ignoring the second-order items, we get

$$dT_T^W = dT_B^W T_A^B T_T^A + T_B^W (T_A^B dT_T^A). \quad (4)$$

According to Paul,¹⁵ an error matrix can be rewritten as

$$dT = T \delta T, \quad (5)$$

where δT is expressed as

$$\delta T = \begin{bmatrix} 0 & -\delta z & \delta y & dx \\ \delta z & 0 & -\delta x & dy \\ -\delta y & \delta x & 0 & dz \\ 0 & 0 & 0 & 0 \end{bmatrix}. \quad (6)$$

In Eq. (6), dx , dy , and dz are translational errors, while δx , δy , and δz are the rotational errors. More details of the derivation of δT can be found in Paul's book¹⁵ as well as in the book by Mooring *et al.*¹⁶

Using Eq. (5) to rewrite Eq. (4) produces

$$T_T^W \delta T_T^W = T_T^W ((T_A^B T_T^A)^{-1} \delta T_B^W T_A^B T_T^A + \delta T_T^A). \quad (7)$$

Let

$$U = T_A^B T_T^A. \quad (8)$$

Then Eq. (7) is simplified as

$$\delta T_T^W = U^{-1} \delta T_B^W U + \delta T_T^A. \quad (9)$$

It is noted that U is in the form of

$$U = \begin{bmatrix} \mathbf{n}_u & \mathbf{o}_u & \mathbf{a}_u & \mathbf{r}_u \\ 0 & 0 & 0 & 1 \end{bmatrix}, \quad (10)$$

where \mathbf{n}_u , \mathbf{o}_u and \mathbf{a}_u are orthogonal unit vectors, while \mathbf{r}_u is the translation vector of U .

Based on Eq. (6), we rewrite δT_T^W , δT_B^W and δT_T^A as

$$\delta T_T^W = \begin{bmatrix} 0 & -\delta z & \delta y & dx \\ \delta z & 0 & -\delta x & dy \\ -\delta y & \delta x & 0 & dz \\ 0 & 0 & 0 & 0 \end{bmatrix}, \quad (11)$$

$$\delta T_B^W = \begin{bmatrix} 0 & -\delta z_b & \delta y_b & dx_b \\ \delta z_b & 0 & -\delta x_b & dy_b \\ -\delta y_b & \delta x_b & 0 & dz_b \\ 0 & 0 & 0 & 0 \end{bmatrix}, \quad (12)$$

$$\delta T_T^A = \begin{bmatrix} 0 & -\delta z_a & \delta y_a & dx_a \\ \delta z_a & 0 & -\delta x_a & dy_a \\ -\delta y_a & \delta x_a & 0 & dz_a \\ 0 & 0 & 0 & 0 \end{bmatrix}, \quad (13)$$

where $(dx_a, dy_a, dz_a, \delta x_a, \delta y_a, \delta z_a)$ and $(dx_b, dy_b, dz_b, \delta x_b, \delta y_b, \delta z_b)$ are the translational and rotational errors of T_T^A and T_B^W , respectively.

Letting $\mathbf{d}_b = [dx_b, dy_b, dz_b]^T$ and $\delta_b = [\delta x_b, \delta y_b, \delta z_b]^T$, the triple product of matrices $U^{-1} \delta T_B^W U$ is equal to

$$U^{-1} \delta T_B^W U = \begin{bmatrix} 0 & -\delta_b \cdot \mathbf{a}_u & \delta_b \cdot \mathbf{o}_u & \delta_b \cdot (\mathbf{r}_u \times \mathbf{n}_u) + \mathbf{d}_b \cdot \mathbf{n}_u \\ \delta_b \cdot \mathbf{a}_u & 0 & -\delta_b \cdot \mathbf{n}_u & \delta_b \cdot (\mathbf{r}_u \times \mathbf{o}_u) + \mathbf{d}_b \cdot \mathbf{o}_u \\ -\delta_b \cdot \mathbf{o}_u & \delta_b \cdot \mathbf{n}_u & 0 & \delta_b \cdot (\mathbf{r}_u \times \mathbf{a}_u) + \mathbf{d}_b \cdot \mathbf{a}_u \\ 0 & 0 & 0 & 0 \end{bmatrix}. \quad (14)$$

From Eqs. (9), (11), (13) and (14), we build the following equations:

$$\begin{aligned} dx &= \delta_b \cdot (\mathbf{r}_u \times \mathbf{n}_u) + \mathbf{d}_b \cdot \mathbf{n}_u + dx_a, \\ dy &= \delta_b \cdot (\mathbf{r}_u \times \mathbf{o}_u) + \mathbf{d}_b \cdot \mathbf{o}_u + dy_a, \\ dz &= \delta_b \cdot (\mathbf{r}_u \times \mathbf{a}_u) + \mathbf{d}_b \cdot \mathbf{a}_u + dz_a, \\ \delta x &= \delta_b \cdot \mathbf{n}_u + \delta x_a, \\ \delta y &= \delta_b \cdot \mathbf{o}_u + \delta y_a, \\ \delta z &= \delta_b \cdot \mathbf{a}_u + \delta z_a. \end{aligned} \quad (15)$$

By using

$$R_u = [\mathbf{n}_u, \mathbf{o}_u, \mathbf{a}_u]^T, \quad (16)$$

$$C_u = [\mathbf{r}_u \times \mathbf{n}_u, \mathbf{r}_u \times \mathbf{o}_u, \mathbf{r}_u \times \mathbf{a}_u]^T, \quad (17)$$

$$\mathbf{d}_b = [dx_b, dy_b, dz_b]^T, \quad (18)$$

$$\delta_b = [\delta x_b, \delta y_b, \delta z_b]^T, \quad (19)$$

Eq. (15) can be expressed in matrix form as

$$\begin{bmatrix} \mathbf{d} \\ \delta \end{bmatrix} = \begin{bmatrix} R_u & C_u & I_{3 \times 3} & O_{3 \times 3} \\ O_{3 \times 3} & R_u & O_{3 \times 3} & I_{3 \times 3} \end{bmatrix} \begin{bmatrix} \mathbf{d}_b \\ \delta_b \\ \mathbf{d}_a \\ \delta_a \end{bmatrix}, \quad (20)$$

where I stands for the identity matrix and O for the zero matrix.

The error equation (20) is further simplified as

$$\mathbf{x} = \mathbf{J}\mathbf{y}, \quad (21)$$

where $\mathbf{x} = [\mathbf{d}, \delta]^T$ is a 6×1 column vector and $\mathbf{y} = [\mathbf{d}_b, \delta_b, \mathbf{d}_a, \delta_a]^T$ is a 12×1 column vector. With this equation, the base and tool calibration can be conducted. Given a sequence of pose measurements $\mathbf{x}(k)$, $k = 1, \dots, n$ ($n \geq 3$), with respect to the linear mapping matrix $\mathbf{J}(k)$, the differential displacement \mathbf{y} at the base and the tool end can be identified by least-square method.

4. POSE ERROR CALCULATION

The pose error \mathbf{x} in Eq. (21) is equal to the difference between the measured and calculated value of end-effector pose,

$$\mathbf{x} = \mathbf{p}_m - \mathbf{p}_c. \quad (22)$$

In the task space of parallel manipulator, tool pose is described by a six-dimensional vector which consists of its Cartesian coordinates of the origin of tool frame and three consecutive rotations about X , Y and Z axes of the reference frame:

$$\mathbf{p} = [x, y, z, \theta_x, \theta_y, \theta_z]^T. \quad (23)$$

For convenience, the pose is divided into two parts: tool position $\mathbf{r} = [x, y, z]^T$ and orientation $\alpha = [\theta_x, \theta_y, \theta_z]^T$.

The coordinates transformation from frame T to the world frame is

$$T_T^W = \begin{bmatrix} \mathbf{Q} & \mathbf{r} \\ 0 & 1 \end{bmatrix}, \quad (24)$$

where

$$\mathbf{Q} = [\mathbf{n}, \mathbf{o}, \mathbf{a}]. \quad (25)$$

Here, \mathbf{n} , \mathbf{o} and \mathbf{a} are unit vectors pointing to the direction of the tool-related frame axes, X_t , Y_t and Z_t , respectively, when viewed in the world frame.

In the meantime, the rotation matrix according to the three rotations is

$$\mathbf{Q} = R_x(\theta_x)R_y(\theta_y)R_z(\theta_z), \quad (26)$$

where

$$R_x(\theta_x) = \begin{bmatrix} 1 & 0 & 0 \\ 0 & c\theta_y & -s\theta_y \\ 0 & s\theta_y & c\theta_y \end{bmatrix},$$

$$R_y(\theta_y) = \begin{bmatrix} c\theta_y & 0 & s\theta_y \\ 0 & 1 & 0 \\ -s\theta_y & 0 & c\theta_y \end{bmatrix}, \quad (27)$$

$$R_z(\theta_z) = \begin{bmatrix} c\theta_z & -s\theta_z & 0 \\ s\theta_z & c\theta_z & 0 \\ 0 & 0 & 1 \end{bmatrix}.$$

Here s and c stand for trigonometric functions \sin and \cos , respectively.

The rotation matrix \mathbf{Q} finally is

$$\begin{bmatrix} c\theta_y c\theta_z & -c\theta_y s\theta_z & s\theta_y \\ s\theta_x s\theta_y c\theta_z + c\theta_x s\theta_z & -s\theta_x s\theta_y s\theta_z + c\theta_x c\theta_z & -s\theta_x c\theta_y \\ -c\theta_x s\theta_y c\theta_z + s\theta_x s\theta_z & c\theta_x s\theta_y s\theta_z + s\theta_x c\theta_z & c\theta_x c\theta_y \end{bmatrix}. \quad (28)$$

From Eqs. (25), (27) and (28), all three rotation angles are obtained as

$$\theta_x = \text{atan2}(-\mathbf{a}_y, \mathbf{a}_z),$$

$$\theta_y = \text{atan2}(\mathbf{a}_x, -\mathbf{a}_y s\theta_x + \mathbf{a}_z c\theta_x), \quad (29)$$

$$\theta_z = \text{atan2}(\mathbf{n}_y c\theta_x + \mathbf{n}_z s\theta_x, \mathbf{o}_y c\theta_x + \mathbf{o}_z s\theta_x),$$

where atan2 is a two-argument arctangent function that yields one unique angle solution. With Eq. (29), we can express the end-effector pose by

$$\mathbf{p} = [\mathbf{r}, \alpha]^T = f(\mathbf{Q}, \mathbf{r}). \quad (30)$$

Accordingly, the measured pose and calculated pose are

$$\mathbf{p}_m = f(\mathbf{Q}_m, \mathbf{r}_m), \quad (31)$$

$$\mathbf{p}_c = f(\mathbf{Q}_c, \mathbf{r}_c). \quad (32)$$

The nominal rotation \mathbf{Q}_c and translation \mathbf{r}_c are calculated from all transformation matrices. For the actual rotation and translation, they cannot be ob-

tained directly with the available measurement instruments. Kinematic calculation is required for such a pose measurement.

5. POSE MEASUREMENT

5.1. Measurement by OPTOTRAK 3020

In this work, the pose measurement is done with OPTOTRAK 3020, a commercial 3D motion and position measurement system of NDI Corp. It consists of infra-red light-emitting diode markers (IREDs) and lateral-effect photodiode cameras.¹⁷ The cameras track the positions of the IRED markers placed on a rigid body to determine the object's position and orientation in its measuring frame. The measurement system has an accuracy to 0.1 mm and resolution to 0.01 mm. By simultaneously tracking more than 256 markers, the system can detect displacements in 6 DOFs in complex applications. So far, such a system has been used for pose measurement¹⁸ and serial manipulator's calibration.¹⁹

In measuring the tool pose in our parallel manipulator system, the first thing to do is to set up a local frame for each object to be measured. We used two group of IRED markers attached to the base and drill holder separately, as shown in Figure 3, to determine the world frame and tool frame. For each

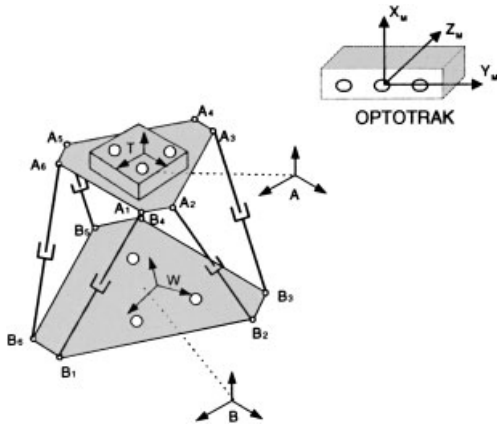


Figure 3. Measurement setup for medical parallel manipulator calibration. Round-shaped objects are IRED markers.

group of three IRED markers, their centroid and a vector normal to the plane passing through them are calculated. The origin of a local frame (tool or world) is located at the centroid, while Z axis is parallel to the normal vector and points upwards. Of the three markers of tool frame, two are intentionally aligned to the desired direction, which is the moving direction of the drilling tool in our work, to determine the X axis.

The readings from OPTOTRAK are the 3D position information of all IRED markers in the measuring frame. We used this information to calculate the position $\mathbf{r}_m = [x, y, z]^T$ of the origin of the tool frame and further to work out its orientation $\alpha_m = [\theta_x, \theta_y, \theta_z]^T$.

5.2. Pose Calculation

Let \mathbf{n}_t , \mathbf{o}_t and \mathbf{a}_t be unit vectors pointing to the direction of the tool-related coordinate axes, X_t , Y_t and Z_t , respectively, with respect to frame M . The coordinates transformation from frame T to the measuring frame is

$$T_T^M = \begin{bmatrix} \mathbf{Q}_t & \mathbf{r}_t \\ 0 & 1 \end{bmatrix}, \quad (33)$$

where

$$\mathbf{Q}_t = [\mathbf{n}_t, \mathbf{o}_t, \mathbf{a}_t] \quad (34)$$

and

$$\mathbf{r}_t = [x_t, y_t, z_t]^T. \quad (35)$$

Similarly, the transformation from frame W to the measuring frame is

$$T_W^M = \begin{bmatrix} \mathbf{Q}_w & \mathbf{r}_w \\ 0 & 1 \end{bmatrix}. \quad (36)$$

The transformation from frame W to T is obtained as

$$T_T^W = (T_W^M)^{-1} T_T^M. \quad (37)$$

From Eq. (36), we get

$$(T_W^M)^{-1} = \begin{bmatrix} \mathbf{Q}_w^T & -\mathbf{Q}_w^T \mathbf{r}_w \\ 0 & 1 \end{bmatrix}. \quad (38)$$

Finally, we get

$$T_T^W = \begin{bmatrix} \mathbf{Q}_w^T \mathbf{Q}_t & \mathbf{Q}_w^T (\mathbf{r}_t - \mathbf{r}_w) \\ 0 & 1 \end{bmatrix}. \quad (39)$$

The rotation and translation are

$$\mathbf{r}_m = \mathbf{Q}_w^T (\mathbf{r}_t - \mathbf{r}_w), \quad (40)$$

$$\mathbf{Q}_m = \mathbf{Q}_w^T \mathbf{Q}_t. \quad (41)$$

With Eq. (31), the measured pose \mathbf{p}_m is obtained.

6. IMPLEMENTATION

The calibration is implemented as an iterative course. First, least squares method is used to solve the linear equations of Eq. (21). The solutions, standing for the errors in the tool and base, are used to modify the estimate of tool and base transformations. The modified matrices are reused to calculate pose error. This course is conducted iteratively until the pose error is small enough to meet a termination condition. In evaluating pose error, two parameters are used: RMSPE and RMSOE, which are the root mean square position and orientation errors defined as

Table I. Preset values of errors (m or rad).

	dx	dy	dz	δ_x	δ_y	δ_z
T_B^W	0.008	0.001	-0.004	0.02	0.01	0.005
T_T^W	0.007	0.002	-0.006	0.03	0.04	0.001

$$\text{RMSPE} = \sqrt{\frac{1}{n} \sum \|\mathbf{d}(k)\|^2}, \quad (42)$$

$$\text{RMSOE} = \sqrt{\frac{1}{n} \sum \|\delta(k)\|^2}.$$

In detail, the calibration procedure is described below.

Step 1: Let the manipulator move to n different poses. For each pose $\mathbf{p}(k)$, obtain the actual tool pose \mathbf{p}_m by Eqs. (31), (40) and (41).

Step 2: Calculate the nominal tool pose \mathbf{p}_c in the world frame according to Eqs. (1), (2) and (32).

Step 3: Calculate the difference between the actual value and the nominal results:

$$\mathbf{x}(k) = \mathbf{p}_m(k) - \mathbf{p}_c(k), \quad k = 1, \dots, n. \quad (43)$$

Step 4: Solve Eq. (21) by least-square method to get the base and tool errors.

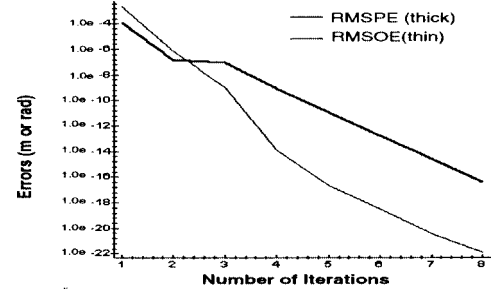
Step 5: Use the base and tool errors to update transformation matrices by

$$T_B^W \leftarrow T_B^W (I + \delta T_B^W), \quad (44)$$

$$T_T^A \leftarrow T_T^A (I + \delta T_T^A). \quad (45)$$

Table II. Manipulator poses of simulations (m or rad).

No.	x	y	z	θ_x	θ_y	θ_z
1	0.005	0.0	0.0	0.0	0.0	0.0
2	0.005	0.0	0.0	0.0872	0.0	0.0
3	0.005	0.005	0.0	0.0872	0.0	0.0
4	0.005	0.005	0.0	0.0872	0.0523	0.0
5	0.005	0.005	0.003	0.0872	0.0523	0.0
6	0.005	0.005	0.003	0.0872	0.0523	0.0349


Figure 4. Pose error versus number of iteration in simulation.

The updated matrices should be made unit magnitude.

Step 6: Check the termination condition. If pose error is small enough, then stop. Otherwise, go to **Step 2**.

7. SIMULATIONS AND EXPERIMENTS

The calibration algorithm was first tested by simulations. A set of preset pose errors, listed in Table I, was added through Eqs. (1), (44) and (45) to both base and tool transformations, which are thought to be identity matrices before calibration. In using the error model, the pose obtained from transformation with error inside is regarded as measured value, while the pose obtained from transformation without error is the nominal value. In simulations, transformations T_A^B were generated with Eq. (2) according to variables given in Table II.

The simulation results are presented in Figure 4 and Tables III and IV. As an iterative process, pose errors of each iteration in the simulation are depicted in Figure 4. It is seen that the pose error reduces exponentially when the number of iteration increases. The transformation can quickly converge to a stable value with our developed error model. In fact, the simulation can obtain very good results ($\text{RMSPE} < 1.0 \times 10^{-5}$ m and $\text{RMSOE} < 5.0 \times 10^{-5}$ rad) after five iterations, as listed in Table III.

Table III. Pose errors of simulation (m or rad).

	No.				
	1	2	3	4	5
RMSPE	0.020080	0.001110	0.000863	0.000115	0.000018
RMSOE	0.071003	0.002122	0.000126	0.000001	0.000000

Table IV. Simulated calibration results.

T_B^W	=	$\begin{bmatrix} 0.999\ 93 & -0.004\ 99 & 0.009\ 99 & 0.007\ 99 \\ 0.005\ 19 & 0.999\ 78 & -0.019\ 99 & 0.001\ 00 \\ -0.009\ 89 & 0.020\ 04 & 0.999\ 75 & -0.003\ 99 \\ 0 & 0 & 0 & 1 \end{bmatrix}$
		$\begin{bmatrix} 0.999\ 19 & -0.000\ 99 & 0.039\ 98 & 0.007\ 00 \\ 0.002\ 19 & 0.999\ 54 & -0.029\ 97 & 0.001\ 99 \\ -0.039\ 94 & 0.030\ 03 & 0.998\ 75 & -0.006\ 00 \\ 0 & 0 & 0 & 1 \end{bmatrix}$

The tool calibration result in simulation is listed in Table IV. It is directly seen that the position errors are fully identified. A calculation based on the rotation matrix also found that the orientation errors are identified too.

After verification by simulations, the calibration method was applied to our parallel manipulator system to calibrate the tool and base transformations. Considering the existence of noise in the measurements, we measured a total of 60 poses in order to eliminate the noise influence. Based on the simulation results, we set the iteration number to 20, which guarantees a convergence value for each matrix. The base and tool calibration results are shown in Table V. The position and orientation errors are reduced to 0.000 07 m (RMSPE) and 0.000 58 rad (RMSOE), respectively.

To understand the effect of the number of measured poses on the accuracy, calibrations were conducted for different groups containing measured poses varied from 5 to 60. For each group, the cali-

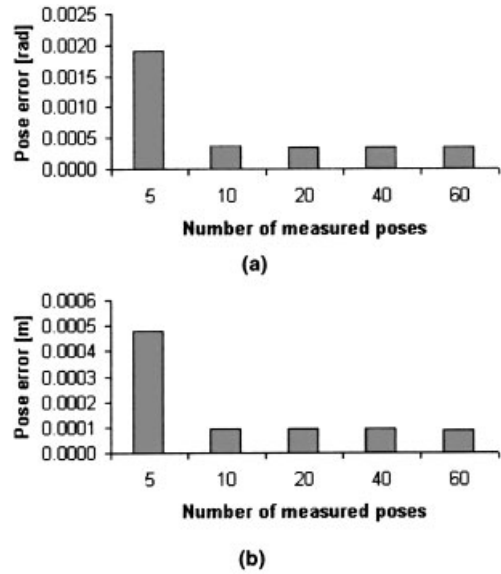


Figure 5. Accuracy versus number of measurements.

bration results were tested against another 60 measured poses. Specifically, manipulator poses were calculated for each measured pose by using transformations based on calibrated matrices. Since the calibrated matrices are different, the pose error will vary with the number of measured pose. Based on the experiment results, the variation is plotted as Figure 5. It is seen that the error is less than 0.1 mm, which is comparable to the accuracy of OPTOTRAK 3020. It is also shown that a better calibration result is obtained with ten measured poses. Accuracy cannot be improved further with more than ten measured poses.

Table V. Calibration results of base and tool transformation.

	Before	After
T_B^W	$\begin{bmatrix} 1 & 0 & 0 & 0.011 \\ 0 & 1 & 0 & 0.005 \\ 0 & 0 & 1 & -0.007 \\ 0 & 0 & 0 & 1 \end{bmatrix}$	$\begin{bmatrix} 0.999\ 96 & -0.005\ 29 & 0.006\ 09 & -0.001\ 22 \\ 0.005\ 30 & 0.999\ 98 & -0.001\ 37 & -0.001\ 15 \\ -0.006\ 09 & 0.001\ 40 & 0.999\ 98 & -0.001\ 91 \\ 0 & 0 & 0 & 1 \end{bmatrix}$
T_T^A	$\begin{bmatrix} 1 & 0 & 0 & 0.008 \\ 0 & 1 & 0 & 0.001 \\ 0 & 0 & 1 & 0.020 \\ 0 & 0 & 0 & 1 \end{bmatrix}$	$\begin{bmatrix} 0.999\ 64 & -0.026\ 28 & -0.004\ 47 & -0.000\ 92 \\ 0.026\ 26 & 0.999\ 64 & -0.003\ 52 & -0.000\ 67 \\ 0.004\ 56 & 0.003\ 41 & 0.999\ 98 & 0.030\ 49 \\ 0 & 0 & 0 & 1 \end{bmatrix}$
Accuracy ^a	[2.61e-2, 3.20e-2]	[7.08e-5, 5.83e-4]

^a[RMSPE,RMSOE].

8. DISCUSSIONS AND CONCLUSIONS

The calibration and measurement technology with an optical position sensor, OPTOTRAK 3020, is described. An error model was established to describe the calibration errors of parallel manipulator with respect to the base and tool transformation. Applying this model in the identification of the two transformation matrices, the accuracy of end-effector motion is significantly improved.

The experiment result shows that the accuracy of calibration can reach 0.1 mm. It is noted that such an accuracy is obtained comparable to that of OPTOTRAK 3020. The authors believe that the error model can be used for other parallel applications with a higher accuracy, providing more advanced measuring technology.

The tool frame was directly set on the tool holder based on IRED coordinates in this work for verifying the calibration method. When setting the frame on the tool itself, tip-end position of the tool can be obtained by pivoting program.¹⁷ This means rotating the tool about a fixed end-tip to get a set of IRED points which generates a sphere. By fitting best this set of points, the center of radius of this sphere is worked out. Finally, the tip-end vector is calculated with this center.

In the base and tool calibration, it is assumed that the transformation from base platform to the mobile platform is accurate. The accuracy of self-calibration of parallel manipulator should be higher than that of base and tool calibration. In fact, the parallel manipulator's resolution is as high as 1 μm in its X/Y motion.²⁰ The error resulting from this transformation can be ignored in the context of this work when compared with calibration accuracy of 0.1 mm.

REFERENCES

1. M. Ceccarelli and M. Sorli, Effects of design parameters on the workspace of a Turin parallel robot, *Int J Robot Res* 17:(8) (1998), 886–902.
2. C. Gosselin, Determination of the workspace of 6-dof parallel manipulators, *ASME J Mech Design* 112:(3) (1990), 331–336.
3. O. Ma and J. Angeles, Architecture singularities of platform manipulator, *IEEE Int Conf on Robotics and Automation*, 1991, pp. 1542–1547.
4. J-P. Merlet, Determination of 6d workspaces of Gough-type parallel manipulator and comparison between different geometries, *Int J Robot Res* 18:(9) (1999), 902–916.
5. P. Nanua, K.J. Waldron, and V. Murthy, Direct kinematic solution of a Stewart platform, *IEEE Trans Robo Autom*, 6:(4) (1990), 438–444.
6. G. Brandt, A. Zimolong *et al.*, Crigos: a compact robot for image-guided orthopedic surgery, *IEEE Trans Info Technol Biomed* 3:(4) (1999), 252–260.
7. S. Bai, M. Y. Teo, W. S. Ng, and C. Sim, Workspace analysis of a parallel manipulator with one redundant dof for skull base surgery, *Proc of IEEE/RSJ Int Conf on Intelligent Robots and Systems (IROS 2001)*, Hawaii, USA, 2001, pp. 1694–1699.
8. C.G. Iurascu and F.C. Park, Geometric algorithms for closed chain kinematic calibration, *IEEE Int Conf on Robotics and Automation*, 1999, pp. 1752–1757.
9. H. Zhuang, O. Masory, and J. Yan, Kinematic calibration of stewart platform using pose measurements obtained by single theodolite, in *Proc of IEEE/RSJ Int Conf on Intelligent Robots and Systems (IROS)*, Pittsburgh, PA, 1995, pp. 329–334.
10. A. Nahvi, J.M. Hollerbach, and V. Hayward, Closed-loop kinematic calibration of a parallel-drive shoulder joint, *IEEE Int Conf on Robotics and Automation*, 1994, pp. 407–412.
11. C.W. Wampler, J.M. Hollerbach, and T. Arai, An implicit loop method for kinematic calibration and its application to closed-chain mechanisms, *IEEE Trans Robo Autom* 11:(5) (1995), 710–724.
12. F.C. Park and B.J. Martin, Robot sensor calibration solving $AX=XB$ on the euclidean group, *IEEE Trans Robo Autom* 10:(5) (1994), 717–721.
13. G. Yang, I-M. Chen, W.K. Lim, and S.H. Yeo, Simultaneous base and tool calibration of a self-calibrated modular parallel robot, *Proc of Int Conf on Control, Automation, Robotics, and Vision*, Singapore, 2000, pp. 489–493.
14. H. Zhuang, Z.S. Roth, and R. Sudhakar, Simultaneous robot/world and tool/flange calibration by solving homogeneous transformation equations of the form $AX=YB$, *IEEE Trans Robo Autom* 10:(4) (1994), 549–554.
15. R.P. Paul, *Robot manipulators mathematics programming and control*, MIT, Cambridge, MA, 1981.
16. B.W. Mooring, Z.S. Roth, and M.R. Driels, *Fundamentals of manipulator calibration*, Wiley, New York, 1991.
17. OPTOTRCK collect guide (Version 1.0.1), Northern Digital Inc., Waterloo, Canada, 1994.
18. Q. Li, L. Zamorano, Z. Jiang, J. Gong, and F. Diaz, Quantitative comparison of the application accuracy between NDI and IGT tracking systems, *Proc of the Biomedical Diagnostic, Guidance, and Surgical-Assist Systems*, San Jose, CA, 1999, pp. 38–48.
19. J.M. Hollerbach and D.J. Bennett, Automatic kinematic calibration using a motion tracking systems, *Robotics Research: the Fourth International Symposium*, edited by R. Bolles and B. Roth, MIT, Cambridge, MA, 1988, pp. 191–198.
20. Operating Manual MS 54E: M-850 HEXAPOD, Physik Instrumente (PI) GmbH, Germany, 1998.